RESEARCH ARTICLE

Check for updates

Insights on the seed selection criteria of SAPO-34 synthesis: structural units and their chemical microenvironment†

Xiaosi Zhang,[a,b] Miao Yang, [ID] *[a] Ye Wang,[a,c] Caiyi Lou,[a,b] Shutao Xu, [ID][a] Peng Tian [ID] *[a] and Zhongmin Liu[a,b]

Seed-assisted synthesis shows great potential to modify the properties of inorganic microporous materials and enhance synthetic efficiency. However, the understanding of the related mechanism is insufficient, especially in silicoaluminophosphate (SAPO) molecular sieve systems. In this work, the seed-assisted synthesis of SAPO-34, an important industrial methanol-to-olefins (MTO) catalyst with **CHA** topology, was investigated by using various seeds with different structures, compositions and morphologies. It reveals that both double 6-ring (**d6r**) units and complex Si environments are key features for a highly effective SAPO seed, which may provide small fragments containing complete or broken **d6r** units with Si–O–Al domains after the dissolution of seeds and thus derive the nucleation and crystallization of SAPO-34. Moreover, small crystal size and high Si content are positive factors for a qualified SAPO seed. Heteronuclear seeds, such as SAPO-18, SAPO-35 and SAPO-56, have been found to be effective for the synthesis of SAPO-34 with improved MTO catalytic performance. For SAPO materials without **d6r** units, their effect strongly depends on the growth solution and there is no preferential phase selectivity for SAPO-34. These findings could prompt the efficient synthesis and property control of SAPO molecular sieves.

Introduction

A seed-assisted method, as a very effective strategy to synthesize inorganic microporous materials, is well acknowledged to enhance the crystallization rate, suppress impurities and tailor physicochemical properties of the product.[1] Many zeolite materials including ZSM-5 (**MFI**),[2,3] beta (***BEA**),[4] mordenite (**MOR**)[5] and ZSM-22 (**TON**)[6] have been synthesized with the assistance of seeds without using any organic structure-directing agent (OSDA). In addition, interzeolite transformation, as an extreme case of seed-assisted crystal growth, supplies an effective pathway to achieve desired zeolites showing huge potential for exploration.[7–12] In recent years, there has been growing interest in seed-assisted synthesis of silicoaluminophosphate (SAPO) molecular sieves.[13–17] As the analogs of zeolites, SAPO molecular sieves have equally important industrial applications.[18–23] In particular, SAPO-34, as an excellent methanol-to-olefins (MTO) catalyst, has received extensive attention,[24,25] and its catalytic performance has been optimized through the seed-assisted synthesis.[16,26–29] However, it seems that only nanosized SAPO-34 seeds[30,31] or ball-milled SAPO-34 seeds with low crystallinity[15,26,28,32–34] are feasible. Conventional SAPO-34 cannot achieve the desired seeded effects.[35] It is highly desirable to understand the seeded behaviour so that a wise protocol on seed selection can be provided for the synthesis of SAPO materials. This is also believed to be favourable for promoting the creation of novel SAPO materials.

In fact, the seed-assisted crystallization process is quite complex and varies depending on both the type of seeds and the growth solution.[36–38] From the perspective of selecting and matching a seed and a growth solution, the same composite building units (cbus) shared between seeds and crystal products obtained from non-seeded growth solutions were proposed to be crucial for seeded synthesis.[37] This structural similarity concept was consequently extended to more basic subunits, such as n-rings, in interzeolite transformation processes.[39,40] However, there have only been a few studies involving heteronuclear seeds due to insufficient recognition of the related principle.[17,41–43] A recent result of the seed-

[a]National Engineering Research Center of Lower-Carbon Catalysis Technology, Dalian National Laboratory for Clean Energy, iChEM (Collaborative Innovation Center of Chemistry for Energy Materials), Dalian Institute of Chemical Physics, Chinese Academy of Sciences, Dalian 116023, P. R. China.
E-mail: yangmiao@dicp.ac.cn, tianpeng@dicp.ac.cn
[b]University of Chinese Academy of Sciences, Beijing 100049, P. R. China
[c]Green Catalysis Centre, College of Chemistry, Zhengzhou University, Zhengzhou 450001, P. R. China
†Electronic supplementary information (ESI) available. See DOI: https://doi.org/10.1039/d3qi00646h

assisted synthesis of zeolite Y revealed that only partial dissolution with solid residue is crucial for a qualified seed, where hydrogel microparticles migrate and attach, inducing fast nucleation and crystal growth.[44] But the working mechanism of a seed in a SAPO system has been rarely investigated.[45,46] Regarding the crystallization mechanism of SAPO-34, Huang *et al.* concluded that the crystal growth of SAPO-34 follows the "birth and spread" mechanism where the nucleus size is about 22 nm corresponding to *ca.* 23 layers of double 6-rings (***d6r***s).[47–49] Hong *et al.* believed that the nucleation of SAPO-34 begins with the formation of a larger ***cha*** cage rather than small cbus.[50] What kind of seed can promote the nucleation and quicken the crystallization of SAPO-34 is still an open question.

In this work, the seeding roles were systematically studied in a conventional morpholine (MOR)-templated hydrothermal synthesis system. The existence of dynamic competition between SAPO-5 and SAPO-34 in this non-seeded growth solution allows us to quickly judge whether the seed works or not, where various materials with different crystal structures, compositions and crystal morphologies were tested as seeds. The working mechanism of the seed in the SAPO synthesis system is proposed, and many alternative and efficient seeds for SAPO-34 synthesis have been found. Our findings provide important insights into the seed-assisted protocol, as well as useful guidance on the rational synthesis of SAPO materials.

Experimental section

Materials and reagents

The chemical reagents used in the experiments included pseudo-boehmite (66.5 wt%), aluminum isopropoxide (Al$(C_3H_7O)_3$, AIP, Aladdin, 98 wt%), distilled water, phosphoric acid (80 wt%), silica sol (27.3 wt%), tetraethylorthosilicate (TEOS, Tianjin Kemiou Chemical Reagent Co. Ltd, 28 wt% SiO_2), fumed silica (FS, Shenyang Chemical Co. Ltd, 100 wt% SiO_2), morpholine (C_4H_9NO, MOR, Guoyao Chemical Reagent Factory, ≥99 wt%), triethylamine ($C_6H_{15}N$, TEA, Tianjin Damao Chemical Reagent Co., 99 wt%), diethylamine ($C_4H_{11}N$, DEA, Tianjin Damao Chemical Reagent Factory, 99 wt%), dipropylamine ($C_6H_{15}N$, DPA, Guoyao Chemical Reagent Factory, ≥98 wt%), *N,N,N*-trimethyl-1-adamantammonium hydroxide ($C_{13}H_{25}NO$, TMAdaOH, Annaiji, 20 wt% in H_2O), *N,N,N',N'*-tetramethyl-1,6-hexane diamine ($C_{10}H_{24}N_2$, TMHDA, Aladdin, ≥99 wt%), hexamethylenimine ($C_6H_{13}N$, HMI, Annaiji, 98 wt%), pyridine (C_5H_5N, Py, Tianjin Kemiou Chemical Reagent Co. Ltd, 99.5 wt%), piperazine ($C_4H_{10}N_2$, PIP, Dibo Chemical Reagent Company, 99.5 wt%), *N,N*-diisopropylethylamine ($C_8H_{19}N$, DIEA, Suzhou Highfine Biotech Co., Ltd, 99 wt%), tetramethylammonium hydroxide (TMAOH, Shanghai Annaiji Chemical Reagent Co., 25 wt%), tetraethyl ammonium hydroxide (TEAOH, Runjing Chemical, 35 wt%), tetramethyl ethylenediamine (TMEDA, Aladdin, 98 wt%), *N,N'*-dimethylethylenediamine (DMEDA, Titan, 98 wt%), hydrofluoric acid (HF, Luoyang Chemical Reagent Factory, 40 wt%), hexadecyltrimethyl ammonium bromide ($C_{16}TAB$, Tianjin Damao Chemical Reagent Factory, 99 wt%), octadecyltrimethyl ammonium bromide ($C_{18}TAB$, Tianjin Damao Chemical Reagent Factory, 99 wt%), tetraethylammonium bromide (TEABr, Shanghai Annaiji Chemical Reagent Co. Ltd, 99 wt%) and sodium hydroxide (NaOH, Aladdin, 99.9 wt% NaOH).

Synthesis and preparation of seeds

Various seeds including eight **CHA** type and nine non-**CHA** type materials were synthesized and collected for the follow-up investigation. As seen in Table S1,† the seed samples were named **A**-*x*–*y* so that the information on the crystal phase (**A**), composition (*x*) and crystal size (*y*) can be read easily. Herein, *x* means the molar ratio of Si to T (T = Si + Al + P), and *y* is the crystal size on the micron scale. Some of the samples were synthesized according to references, and some others were self-synthesized. The related information and preparation methods are given in Table S1,† and the XRD patterns, SEM images and element compositions can be found in their mentioned parts.

SAPO-34–BM. The SAPO-34–BM seed was an amorphous SAPO-34 precursor prepared according to our previous work.[32] Typically, 6.0 g of calcined **CHA**-0.20–2 sample was dispersed into 12.0 g of water and milled using a planetary ball mill (QM-3SP2, Nanjing China) with an agate beads mixture of diameters 3, 6 and 10 mm at 550 rpm for 360 min. After milling, the mud was collected and dried at 110 °C overnight.

CHA-0.19–0.5. The typical preparation procedure is as follows: 3.0 g of SAPO-34–BM precursor was put into 12.0 g of 10 wt% DEA aqueous solution. The mixture was placed in a 50 mL Teflon-lined autoclave and statically heated in an oven at 200 °C for 2 h. The product was washed and recovered through centrifugation and then dried at 110 °C overnight. The sample was calcined at 550 °C in air for 4 h to remove the occluded organic species.

MS (CHA-0.19–10, CHA-0–0.5 and CHA-0.10–2). In a typical hydrothermal synthesis procedure, the required amount of aluminum source was first mixed with deionized water. Second, the required amount of phosphate source was added to the mixture under stirring. Then, the required amount of silica source was introduced into the synthesis gel, leaving the mixture under stirring for a certain time period. If necessary, the SAPO-34–BM seed was added to the mixture at this time. The resulting mixture was transferred into a 50 mL Teflon-lined stainless-steel autoclave and heated at an appropriate temperature under rotation for a certain time period. After crystallization, the solid products were filtered and washed with abundant water and dried at 100 °C overnight. The samples were calcined at 550 °C in air for 4 h to remove the occluded organic species.

Unmentioned seeds were synthesized according to the specific methods in the corresponding references.

Synthesis of SAPO-34 molecular sieves

A typical hydrothermal synthesis using MOR as the OSDA was carried out with a gel molar composition of $0.8P_2O_5 : 1.0Al_2O_3 : mSiO_2 : 2.5MOR : 100.0H_2O$ (*m* = 0.6 or 1.0).

Pseudo-boehmite, distilled water, phosphoric acid and silica sol were sequentially added into a plastic beaker. The resulting mixture was stirred at room temperature for 30 min to form a homogeneous gel. After further addition of MOR, the mixture was transferred into a stainless-steel autoclave and sealed quickly. Subsequently, the autoclave was transferred into an oven, heated to 200 °C, and kept for a certain crystallization period under rotation. The product was washed and recovered through centrifugation and dried at 110 °C overnight.

For the seed-assisted synthesis, the gel composition and synthesis procedure were the same as the above except for the addition of seed in the initial gel (5 wt% addition, based on the oxide dry mass). It should be noted that all the seeds used in this work were in calcined form.

The yields of products were calculated using the following equation: yield $= M_{sample} \times 85\%/(M_{seed} + M_{(Al_2O_3+P_2O_5+SiO_2)gel}) \times 100\%$, where M_{sample}, M_{seed} and $M_{(Al_2O_3+P_2O_5+SiO_2)gel}$ stand for the weight of the products, the weight of the added seed and the dry mass of inorganic oxides in the starting mixture, respectively. 85% is the estimated average value of framework compounds included in the samples.

Catalytic test

The performance of the catalysts in the MTO reaction was tested in a quartz tubular fixed-bed reactor under atmospheric pressure. Typically, 0.3 g of calcined SAPO-34 catalysts (sieve fraction, 40–60 mesh) was loaded in a quartz reactor and activated under a nitrogen flow at 550 °C for 1 h. After cooling to the reaction temperature of 450 °C, methanol was fed by switching the carrier gas to pass through the methanol saturator containing methanol at 30 °C, corresponding to a weight hourly space velocity (WHSV) of 3.65 h^{-1}. The products were analysed by an online gas chromatograph (Agilent GC 7890N) equipped with a flame ionization detector (FID) and a Plot-Q column.

Characterization

The powder X-ray diffraction (PXRD) data used for the phase identification were collected on a PANalytical X'Pert PRO X-ray diffractometer using Cu Kα radiation ($\lambda = 1.54059$ Å), operating at 40 kV and 40 mA. The relative crystallinity of SAPO-34 was calculated based on the average peak intensity of the three strongest peaks of SAPO-34 (2 theta = 9.5°, 16.5° and 20.5°).

Scanning electron microscopy (SEM) images were acquired on a Hitachi SU8020 microscope.

The inorganic elemental compositions of the solid samples were measured with a Philips Magix-601 X-ray fluorescence (XRF) spectrometer and a Horiba X-max energy dispersive X-ray (EDX) spectrometer.

The textural properties of the calcined samples were measured by N_2 sorption at −196 °C on a Micromeritics ASAP2020 volumetric adsorption analyser. Prior to the measurement, the sample was degassed at 350 °C under vacuum for 4 h. The total surface area was evaluated based on the BET equation. The micropore surface area and the micropore volume were calculated using the t-plot method.

The solid-state MAS NMR experiments were performed at a wide-bore 11.7 T superconducting magnet on a Bruker Avance NEO 500 spectrometer with a resonance frequency of 99.35 MHz for ^{29}Si. The ^{29}Si MAS NMR spectra were recorded using a 4 mm DVT MAS probe with a spinning rate of 8 kHz using high-power proton decoupling. 4096, 3072 or 2048 scans were accumulated with a π/4 pulse width of 2.5 μs and a 10 s recycle delay. The chemical shifts were referenced to kaolinite at −91.5 ppm.

Results and discussion

The conventional and seed-assisted synthesis of SAPO materials

A conventional MOR-templated SAPO synthesis system with molar composition of $0.8P_2O_5/1.0Al_2O_3/mSiO_2/2.5MOR/100H_2O$ was taken as a non-seeded growth solution to conduct the research. As shown in Table 1, Fig. 1 and Fig. S1,† SAPO-5 appears as a metastable phase at the initial stage, which gradually transforms into SAPO-34. Prolonging the reaction time or increasing the silica dosage quickens the formation of SAPO-34 and enhances the solid yield, but the SAPO-5 competitive phase cannot be eliminated within 8 h. The product morphology of SAPO-34 and SAPO-5 is quite distinctive, and their individual compositions were analyzed by EDX (Table 1). Interestingly, SAPO-34 crystals always have higher silica content than SAPO-5, irrespective of the initial silica dosage. This suggests that the birth and crystal growth of SAPO-34 prefers a silica-rich environment, while the crystallization of SAPO-5 does not. The higher bulk silica content of a product is mainly due to its increased proportion of the SAPO-34 crystalline phase. Both 24 h products, C-0.6–24 h and C-1.0–24 h, are highly crystalline pure SAPO-34 with large crystal sizes over 10 μm and higher silica content over 15%. These results demonstrate a typical crystallization process of a SAPO material where Si atoms enter the solid phase gradually.[51,52] The introduction of Si is the slowest step, which can be seen as a rate-limiting step. It is difficult to control the crystalline phase, crystal size and silica content (acidity) simultaneously because a prolonged reaction time can eliminate impurity, but increase the silica content and crystal size.

Fortunately, a ball-milled SAPO-34 (named SAPO-34–BM, $Al_{0.459}Si_{0.199}P_{0.341}O_2$) has been confirmed to be an efficient seed in our previous work.[15,26,33] When 5 wt% SAPO-34–BM was added to assist the crystallization, pure SAPO-34 was obtained in 8 h. The yield of S-0.6–8 h was up to 89.2% in comparison with 62.2% of C-0.6–8 h. The crystal size of the product decreases and exhibits obvious aggregation (Fig. 1b, S-0.6–8 h). This system is thus an ideal model to quickly judge and compare the role of seeds. Therefore, more seeds have been tested in this system to find more effective seeds and understand how seeds can help with the crystallization of SAPO-34.

Effects of various CHA-type seeds

Three **CHA**-type seeds with different crystal sizes and comparable compositions were first selected, which were designated

Table 1 Synthesis conditions and results from an MOR–templated SAPO system[a]

Sample	m (SiO$_2$)	Product[b]	Yield (%)	XRF	EDX[c] AFI	CHA
C-0.6–2 h	0.6	**AFI** (**CHA**)	44.2	Al$_{0.692}$Si$_{0.048}$P$_{0.261}$O$_2$	0.044	0.102
C-0.6–8 h	0.6	**CHA** (**AFI**)	62.2	Al$_{0.501}$Si$_{0.093}$P$_{0.406}$O$_2$	0.070	0.181
C-0.6–24 h	0.6	**CHA**	93.2	Al$_{0.482}$Si$_{0.155}$P$_{0.363}$O$_2$	—	
C-1.0–2 h	1.0	**CHA** (**AFI**)	45.5	Al$_{0.506}$Si$_{0.079}$P$_{0.415}$O$_2$	0.057	0.106
C-1.0–8 h	1.0	**CHA** (**AFI**)	70.4	Al$_{0.491}$Si$_{0.133}$P$_{0.376}$O$_2$	0.062	0.184
C-1.0–24 h	1.0	**CHA**	87.0	Al$_{0.468}$Si$_{0.191}$P$_{0.341}$O$_2$	—	
S-0.6–2 h	0.6	**CHA** (minor **AFI**)	71.4	Al$_{0.524}$Si$_{0.073}$P$_{0.403}$O$_2$	—	
S-0.6–4 h	0.6	**CHA** (minor **AFI**)	85.1	Al$_{0.488}$Si$_{0.117}$P$_{0.395}$O$_2$	—	
S-0.6–8 h	0.6	**CHA**	89.2	Al$_{0.479}$Si$_{0.159}$P$_{0.362}$O$_2$	—	

[a] Gel molar composition: 0.8P$_2$O$_5$/1.0Al$_2$O$_3$/mSiO$_2$/2.5MOR/100H$_2$O; reaction temperature: 200 °C. The products were designated as C-m–n, where m is the silica dosage and n is the reaction time in hours. When 5 wt% of SAPO-34–BM seed (based on the total mass of oxides in the gel) was added, the products were designated as S-m–n. [b] The impurity is labelled in the parentheses. [c] Si/(Si + Al + P) molar ratio of each crystalline phase determined by EDX.
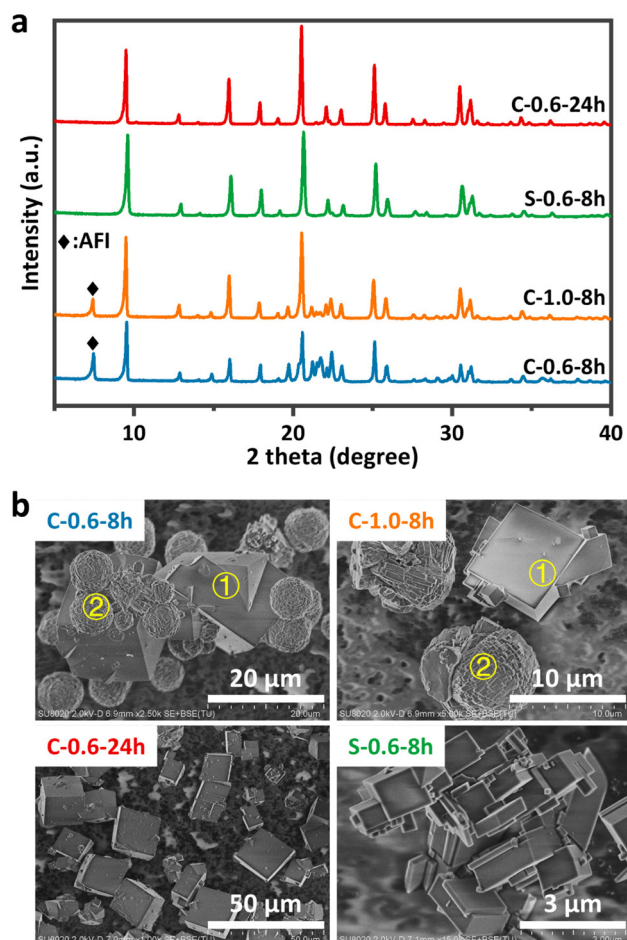

Fig. 1 (a) The powder XRD patterns and (b) SEM images of relevant products. The numbers inserted in b represent different crystal phases. The statistical averages of elemental compositions for C-0.6–8 h: ① Al$_{0.496}$Si$_{0.181}$P$_{0.322}$O$_2$, ② Al$_{0.505}$Si$_{0.070}$P$_{0.426}$O$_2$; C-1.0–8 h: ① Al$_{0.490}$Si$_{0.184}$P$_{0.326}$O$_2$, ② Al$_{0.503}$Si$_{0.062}$P$_{0.435}$O$_2$.

as **CHA**-x–y. Here, x is the Si/T molar ratio (T = Si + Al + P), and y is the crystal size on the micron scale. The corresponding synthesized product was named S$_{\mathbf{CHA}\text{-}x\text{-}y}$. As seen in Fig. 2, **CHA**-0.19–0.5 and **CHA**-0.20–2 with crystal sizes of 0.5 μm and 2 μm, respectively, can effectively inhibit the formation of impurities and produce a pure SAPO-34 product. In contrast, **CHA**-0.19–10 with its larger size exhibits the worst performance. It is speculated that more nucleation centres of SAPO-34 are available for relatively smaller seeds resulting in the pure SAPO-34 product.

The effect of compositions of **CHA**-type seeds was further investigated. The Si/T molar ratios of the selected seeds increase from 0 to 0.91, and their crystal sizes are as small as possible to eliminate the morphology effects. As shown in Fig. 3, when the seeds possess a Si/T molar ratio of 0.15 or higher, they can have an ability in eliminating the SAPO-5 competitive phase. There are lots of SAPO-5 crystals in the SEM images for other cases (Fig. 3 and S2†), even though their solid yields have increased to different degrees. It is noted that the product synthesized with the **CHA**-0.91–0.5 (nanosized SSZ-13) seed contains a small amount of cristobalite phase and its yield is also slightly lower than that of **CHA**-0.15–1, which is supposed to be caused by the relatively low dissolubility of aluminosilicate SSZ-13 in the SAPO gel. The results show that the introduction of solid seeds can accelerate the crystallization rate, while the high-silica SAPO gel is more powerful for avoiding the formation of impurity and prompting the crystallization of SAPO-34.

To understand the working mechanism of the seed, silica-rich SAPO-34 with small crystal size and twinning morphology (**CHA**-0.20–2 seed) was used to monitor its evolution process (Fig. 4). The XRD patterns of the products synthesized without seed and those seeded by **CHA**-0.20–2 are displayed in Fig. S3.† Clearly, with the addition of **CHA**-0.20–2 seed, SAPO-34 begins to form at the very initial stage, and SAPO-5 impurity can be effectively inhibited. There is a steep increase of the solid yield from 0.5 h to 1.5 h (Fig. 4a). The product
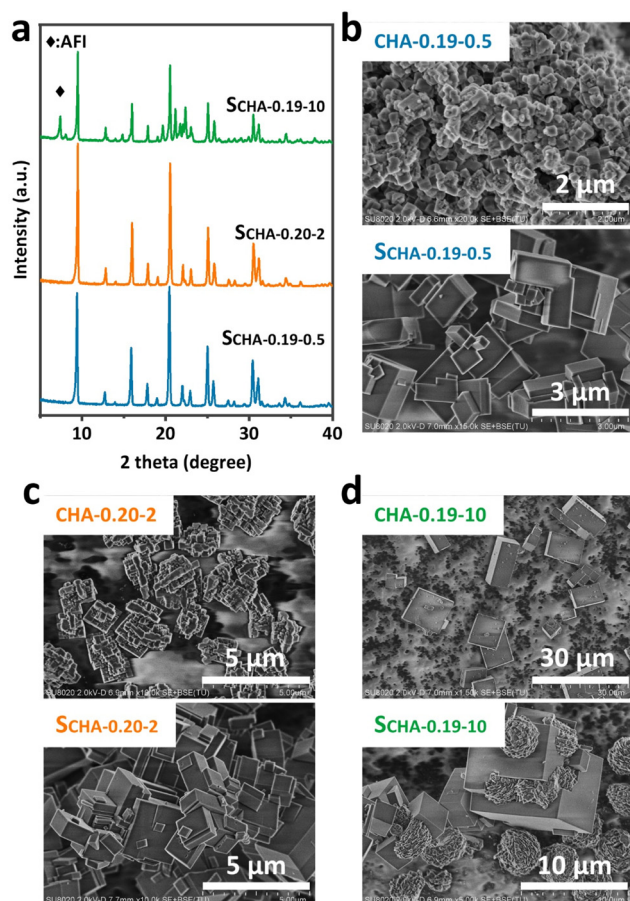
Fig. 2 The effect of crystal sizes of SAPO-34 seeds on the synthesis. (a) The powder XRD patterns of the products, and (b–d) SEM images of the seeds (top) and the corresponding products (bottom). The gel composition and synthesis conditions were the same as those of sample S-0.6–8 h, except for the variation of seeds.

Fig. 3 The effect of composition variation of **CHA**-type seeds on the synthesis. (a) The powder XRD patterns and (b) solid yields of the products, and (c–e) SEM images of the **CHA**-type seeds with different Si contents (top) and the corresponding products (bottom). The gel composition and synthesis conditions were the same as those of sample S-0.6–8 h, except for the variation of seeds.

S$_{CHA-0.20–2}$-1.5 h has a solid yield of 70% with a relative crystallinity of 84%, suggesting the fast crystallization of SAPO-34, while a strong XRD peak at 2θ of 22° appears at around 2 h due to the cristobalite phase (Fig. S3†). This suggests that the crystallization route may be changed by seed addition, where the formation rate of SAPO-34 becomes faster, and part of the inorganic reactants forms a metastable cristobalite phase, which disappears and transfers to pure SAPO-34 after 2 h. Correspondingly, the SEM images show that the size of the seeds becomes smaller, and the crystal edge becomes smooth at 0–1 h, implying a clear dissolution process (Fig. 4b). Meanwhile, new SAPO-34 crystals with clear and regular edges can be found in 1 h, which are surrounded by residual small seeds (in red dotted squares). Subsequently, the product crystals grow up quickly and exhibit an angular but aggregated appearance, which is consistent with a rapid increase of the solid yield. No seeds can be found in the SEM images after 2 h. The relative crystallinity of SAPO-34 reaches 100%, and the solid yield is 91.1% at 4 h. In the case of a blank system without seed, there are no solid products until 1 h of crystalli-
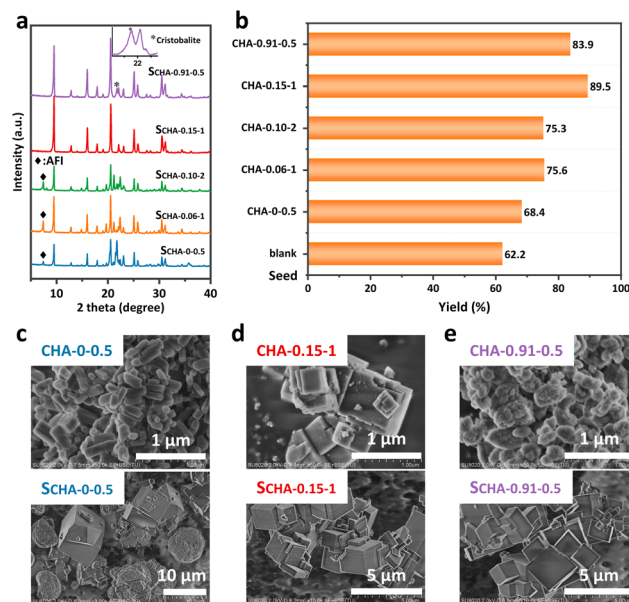
zation (Fig. 4a), and its solid yield was consistently lower than that of the seeded system. The products exhibit the local highest relative crystallinity of *ca.* 71.7% (for SAPO-34 phase) at 4 h, together with the coexistence of a large amount of SAPO-5 impurity. According to the above results, it is believed that the seed dissolves quickly during the crystallization, releasing the structural fragments and/or growth surface that promote the fast crystallization of SAPO-34 and inhibit the formation of SAPO-5 impurity.

Effects of various non-CHA seeds

It is normally believed that the same cbus are necessary for a seed to help the crystallization of target products.[37] But recently, this scenario has often been challenged.[38] What are the required cbus for SAPO-34 seeds? To clarify this question, more SAPO seeds with non-**CHA** structure were tried in this synthesis system. As shown in Scheme 1, the structure of **LEV** (SAPO-35), **AFX** (SAPO-56) and **AEI** (SAPO-18) contains *d6r* units but without a **CHA** cavity, while the structure of **LTA** (SAPO-42), **RHO** (DNL-6) and **SOD** (SAPO-20) possesses 4-, 6- and/or 8-rings but without *d6r* units. Note that two new parameters, the D-measure and a smooth overlap of atomic positions (SOAP), were developed to explain the diffusionless inter-zeolite transition regardless of common cbus shared between the two structures.[53] As seen in Fig. S4,† **LEV**, **AFX** and **AEI** also show a closer relationship with **CHA** than the others.

As seen in Fig. 5, the three seeds with *d6r* units, including **LEV**-0.18–5 (SAPO-35), **AFX**-0.22–8 (SAPO-56) and **AEI**-0.07–1 (SAPO-18), are all very effective in suppressing SAPO-5 impurity

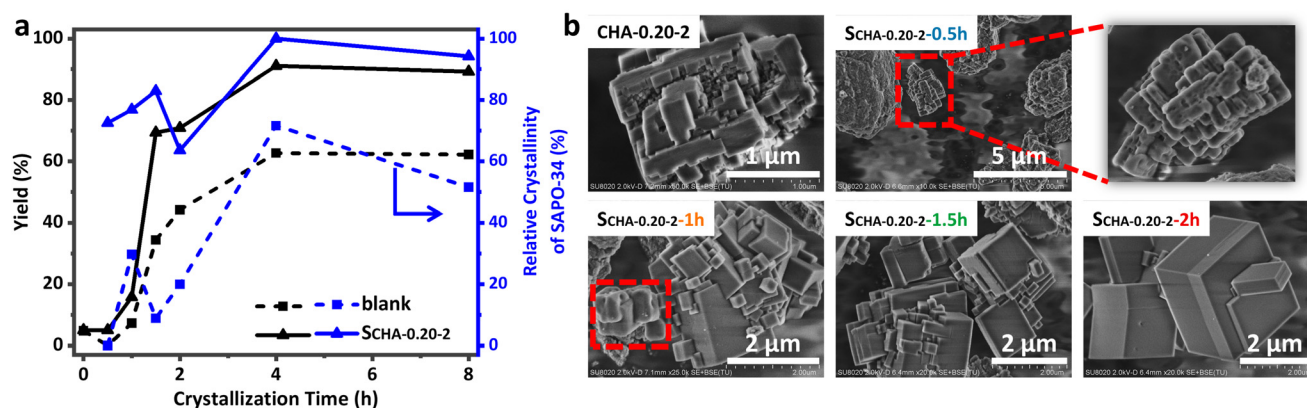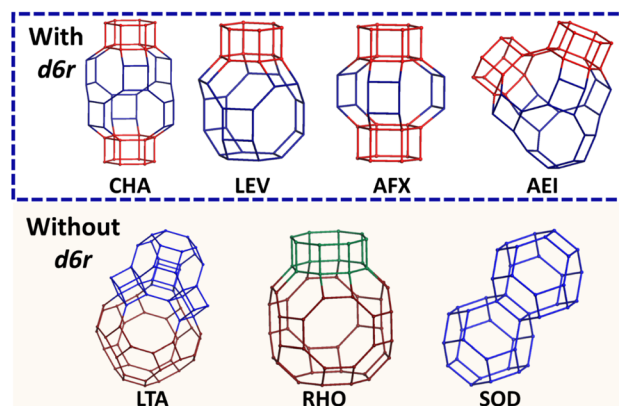**Fig. 4** (a) Solid yields (left axis) and the relative crystallinity (right axis) of the products synthesized without seed and with the **CHA**-0.20−2 seed and (b) SEM images of the seed and the corresponding products with different reaction times. The crystals in the red dotted squares were partially dissolved seeds. The gel composition was the same as that of sample S-0.6−8 h except for the absence of seed for the blank system and the use of **CHA**-0.20−2 seed for S$_{CHA-0.20-2}$.

Scheme 1 The frameworks of the selected seeds with different topologies. (*d6r*, red coloured; *lta* cage, brown coloured; *d8r*, green coloured.)

Fig. 5 The effect of non-**CHA** SAPO seeds containing *d6r* units on the synthesis. (a) The powder XRD patterns and (b) the solid yields of the products, and (c−e) SEM images of various SAPO seeds (top) and the corresponding seed-assisted products (bottom). The gel composition and synthesis conditions were the same as those of sample S-0.6−8 h except for the variation of seeds.

and promoting the crystallization of SAPO-34. The product crystal sizes are obviously smaller than the conventional ones. Their yields are all above 88%, indicating the completion of crystallization. Notably, the crystal size of the S$_{AFX-0.22-8}$ product is the smallest despite the **AFX**-0.22−8 seed presenting a disk morphology with a diameter of over 10 μm. Possibly, the **AFX** disk is quite thin and exposes a larger surface area (60.35 m^2 g^{-1}, Table S2†), which can dissolve easily and supply more growth centres. In addition, **AEI**-0.07−1 performs much better than **CHA**-0.06−1 (Fig. 3a), although it has a comparable silica content and crystal size. However, further attempts using AlPO-18 (**AEI**-0−0.5) and another SAPO-18 with lower Si content (**AEI**-0.03−0.5) as seeds give failure results (Fig. S5†).

All the SAPO seeds without *d6r* units deliver a mixture product of SAPO-34 with impurities and slightly increased solid yields, showing their weak effect as seeds for SAPO-34 synthesis under the present system (Fig. 6). Moreover, by comparing the XRD patterns and solid yields of S$_{RHO-0.33-8}$ and S$_{RHO-0.25-0.5}$, it is clear that high silica-content seeds possess
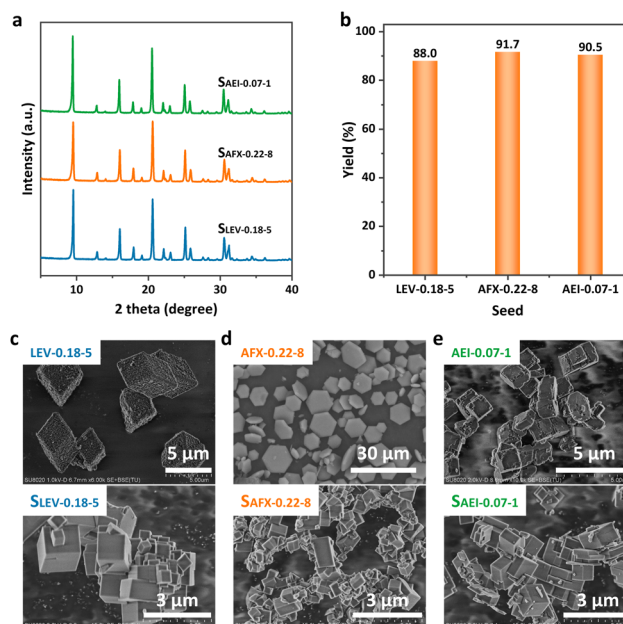
relatively strong ability for inhibiting the impurities and prompting the crystallization of SAPO-34, in agreement with the findings in the aforementioned section. However, it was noted that when a concentrated MOR-templated synthesis system (delivering pure SAPO-34 in the absence of seeds at 2 h)[54] was employed, these seeds can behave with positive effects and quicken the crystallization of SAPO-34 with high purity and high product yield (Fig. S6†). These results imply that the seeded effect of SAPO materials without *d6r* units is
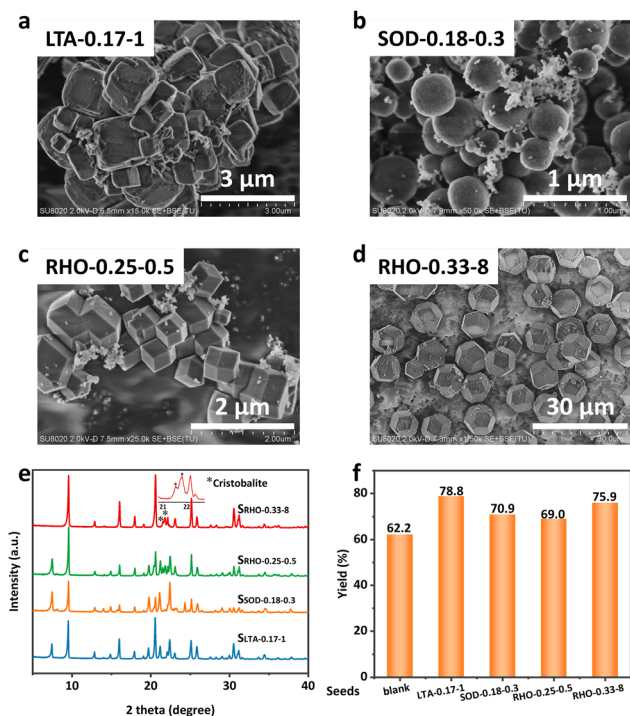
Fig. 6 The effect of non-**CHA** SAPO seeds without **d6r** units on the synthesis. The SEM images of SAPO seeds without **d6r** units (a–d), the powder XRD patterns (e) and solid yields (f) of the corresponding seed-assisted synthesis products. The gel composition and synthesis conditions were the same as those of sample S-0.6–8 h except for the variation of seeds.

Fig. 7 Solid-state ^{29}Si MAS NMR spectra for the calcined SAPO seeds with different topologies.

highly dependent on the growth solution. They have the ability to prompt the crystallization of SAPO molecular sieves, but with inferior phase selectivity for SAPO-34.

Based on the above results, it is concluded that SAPO seeds containing **d6r** units possess superior ability to derive the nucleation and crystallization of SAPO-34. High silica content and small crystal size of the seeds are positive factors for prompting the crystallization of SAPO-34, although they might not be the necessary requirements for a qualified SAPO-34 seed. Possibly, suitable silica environments of the seeds are more important, which are discussed below.

Microscopic chemical environments of various seeds

Solid-state ^{29}Si MAS NMR was employed to investigate the local Si chemical environments. As shown in Fig. 7, all the efficient SAPO seeds with **d6r** units, **AEI**-0.07–1, **CHA**-0.20–2, **AFX**-0.22–8 and **LEV**-0.18–5, exhibit very wide ^{29}Si MAS NMR signals ranging from −90 to −120 ppm, indicating a very complicated Si coordination environment.[51,55] However, the inefficient **CHA**-0.06–1 mainly gives a strong signal at *ca.* −95 ppm, attributed to the Si(4Al) environment.[56] For the seeds without **d6r** units (Fig. S7†), they all possess a certain amount of Si island species, except for the **RHO**-0.25–0.5 seed.

Previous literature studies have demonstrated that the SAPO framework is vulnerable to alkaline treatment, where the Si–O–
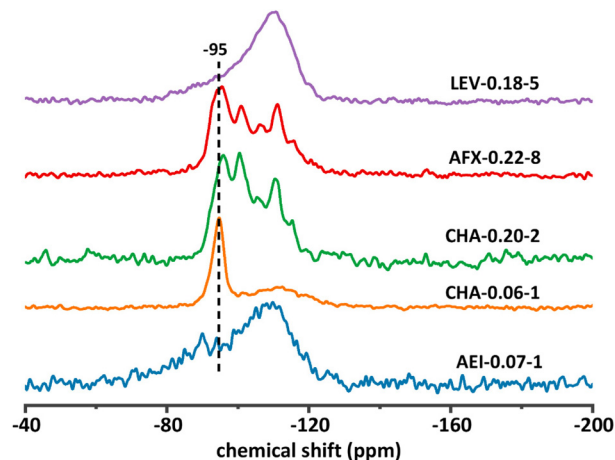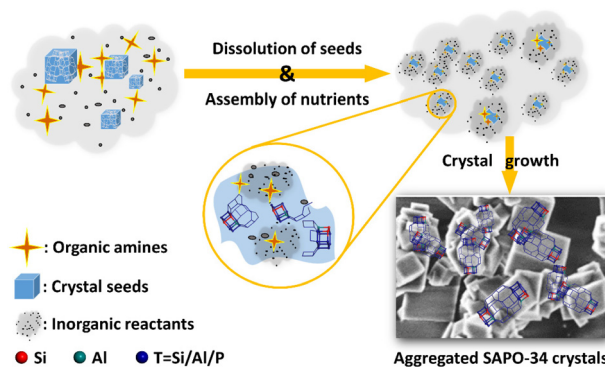
Al domains in Si islands have high stability relative to that of other connections.[57,58] Moreover, our recent work revealed that small fragments enriched with Si–O–Al bonds are critical species for quickening the crystallization of SAPO-34.[54] Their concentration affects the crystallization rate and the ultimate crystal size. Therefore, it is speculated that both **d6r** units and complex Si environments are essential features for a highly effective SAPO seed. The Si–O–Al domains in Si islands of SAPO seeds containing **d6r** units might be largely retained after the dissolution of the seeds and contribute to the nucleation and crystallization of SAPO-34.

A plausible hydrothermal crystallization mechanism is thus proposed based on the above analysis and is illustrated in Scheme 2. In the initial stage, the seeds dissolve and provide small fragments containing complete or broken **d6r** units with Si–O–Al domains. The negative Si–O–Al bonds can have strong interactions with protonated amines and thus initiate fast assembly and bonding of inorganic substances around them under the guidance of an organic template. This process could lead to an increase of gel pH[59] and promote the further dissolution of seed and inorganic sources, which may trigger

Scheme 2 A plausible crystallization mechanism in a seed-assisted synthesis system.

Table 2 Catalytic lifetime^a and the selectivity of C_2H_4 plus C_3H_6 ^{b} of the samples in the MTO reaction (WHSV = 3.65 h^{-1}, T = 450 °C)

Sample	Lifetime (min)	$C_2^=$ (%)	$C_3^=$ (%)	$C_2^= + C_3^=$ (%)	Composition^c
S-0.6–8 h	123	47.5	35.5	83.1	$Al_{0.479}Si_{0.159}P_{0.362}O_2$
$S_{AFX-0.22}$-8 h	157	51.4	37.1	85.5	$Al_{0.491}Si_{0.111}P_{0.398}O_2$
$S_{AEI-0.07-1}$-8 h	157	49.1	37.5	84.5	$Al_{0.487}Si_{0.157}P_{0.322}O_2$

^{a} Catalytic lifetime is defined as the reaction duration with ≥99% methanol conversion. ^{b} The highest selectivity of $C_2^=$ and $C_3^=$ under ≥99% methanol conversion. ^{c} Measured by XRF.

rapid secondary nucleation of SAPO-34. A competitive phase is thus effectively inhibited. Thus, the dissolution of the seeds, the nucleation, the depolymerization of sources and the growth of crystal products take place simultaneously, resulting in fast crystallization processes and formation of small SAPO-34 aggregates.

MTO catalytic performance of seed-synthesized SAPO-34

The MTO catalytic performance of SAPO-34 synthesized with the assistance of these new heteronuclear seeds (Fig. S8†) was evaluated. The textural properties of the selected samples are displayed in Table S3,† which confirm their high crystallinity. The catalytic results are presented in Table 2. For samples S-0.6–8 h and $S_{AEI-0.07-1}$-8 h with similar composition, the shorter catalytic lifetime and lower C_2H_4 plus C_3H_6 selectivity on S-0.6–8 h are supposed to be due to its relatively large crystal size. $S_{AFX-0.22}$-8 h exhibits the best catalytic performance with the highest C_2H_4 plus C_3H_6 selectivity of 85.5%, which should result from its relatively low Si content and small crystal size (~800 nm). The results indicate that heteronuclear SAPO seeds with *d6r* units and complex Si environments are effective seeds to promote the crystallization of SAPO-34 with improved catalytic performance.

Conclusions

In summary, the effects of various seeds on SAPO-34 crystallization have been well investigated and reveal that both *d6r* units and Si–O–Al domains are important for a highly effective SAPO seed. Small Si–O–Al domains in Si islands of SAPO seeds containing *d6r* units might be largely retained after the dissolution of the seeds and contribute to the nucleation and crystallization of SAPO-34. For SAPO seeds without *d6r* units, their effect is dependent on the growth solution. They have the ability to prompt the crystallization of SAPO molecular sieves, but with inferior phase selectivity for SAPO-34. The resultant SAPO-34s synthesized with the assistance of heteronuclear seeds (*e.g.* SAPO-18, SAPO-56) show good catalytic performance in the MTO reaction. The conclusion provides wise seed selection guidance on the synthesis of SAPO-34, which will prompt the development of efficient synthesis strategies for SAPO molecular sieves.

Author contributions

The manuscript was written through contributions from all authors. All authors have given approval to the final version of the manuscript.

Conflicts of interest

There are no conflicts to declare.

Acknowledgements

References

1 R. Jain, A. Mallette and J. Rimer, Controlling Nucleation Pathways in Zeolite Crystallization: Seeding Conceptual Methodologies for Advanced Materials Design, *J. Am. Chem. Soc.*, 2021, **143**, 21446–21460.

2 G. Majano, A. Darwiche, S. Mintova and V. Valtchev, Seed-Induced Crystallization of Nanosized Na-ZSM-5 Crystals, *Ind. Eng. Chem. Res.*, 2009, **48**, 7084–7091.

3 H. Dai, Y. Shen, T. Yang, C. Lee, D. Fu, A. Agarwal, T. T. Le, M. Tsapatsis, J. C. Palmer, B. M. Weckhuysen, P. J. Dauenhauer, X. Zou and J. D. Rimer, Finned zeolite catalysts, *Nat. Mater.*, 2020, **19**, 1074–1080.

4 B. Xie, J. W. Song, L. M. Ren, Y. Y. Ji, J. X. Li and F. S. Xiao, Organotemplate-Free and Fast Route for Synthesizing Beta Zeolite, *Chem. Mater.*, 2008, **20**, 4533–4535.

5 K. P. Cao, D. Fan, S. Zeng, B. H. Fan, N. Chen, M. B. Gao, D. L. Zhu, L. Y. Wang, P. Tian and Z. Liu, Organic-free synthesis of MOR nanoassemblies with excellent DME carbonylation performance, *Chin. J. Catal.*, 2021, **42**, 1468–1477.

6 P. Niu, P. Liu, H. Xi, M. Lin, J. Wang, X. Chen, L. Jia, P. Wang, B. Hou and D. Li, Crystallization Mechanism of Pure-Silica ZSM-22 in the Seed-Assistant System, *Cryst. Growth Des.*, 2018, **18**, 6591–6601.

7 C. M. Zicovich-Wilson, F. Gandara, A. Monge and M. A. Camblor, In Situ Transformation of TON Silica Zeolite into the Less Dense ITW: Structure-Direction Overcoming Framework Instability in the Synthesis of SiO_2 Zeolites, *J. Am. Chem. Soc.*, 2010, **132**, 3461–3471.

8 S. Goel, Z. Wu, S. I. Zones and E. Iglesia, Synthesis and catalytic properties of metal clusters encapsulated within small-pore (SOD, GIS, ANA) zeolites, *J. Am. Chem. Soc.*, 2012, **134**, 17688–17695.

9 S. Goel, S. I. Zones and E. Iglesia, Encapsulation of metal clusters within MFI via interzeolite transformations and direct hydrothermal syntheses and catalytic consequences of their confinement, *J. Am. Chem. Soc.*, 2014, **136**, 15280–15290.

10 S. Goel, S. I. Zones and E. Iglesia, Synthesis of Zeolites via Interzeolite Transformations without Organic Structure-Directing Agents, *Chem. Mater.*, 2015, **27**, 2056–2066.

11 C. G. Li, M. Moliner and A. Corma, Building Zeolites from Precrystallized Units: Nanoscale Architecture, *Angew. Chem., Int. Ed.*, 2018, **57**, 15330–15353.

12 M. J. Mendoza-Castro, E. De Oliveira-Jardim, N. T. Ramirez-Marquez, C. A. Trujillo, N. Linares and J. Garcia-Martinez, Hierarchical Catalysts Prepared by Interzeolite Transformation, *J. Am. Chem. Soc.*, 2022, **144**, 5163–5171.

13 M. Yang, P. Tian, L. Liu, C. Wang, S. Xu, Y. He and Z. Liu, Cationic surfactant-assisted hydrothermal synthesis: an effective way to tune the crystalline phase and morphology of SAPO molecular sieves, *CrystEngComm*, 2015, **17**, 8555–8561.

14 Q. Wu, I. Oduro, Y. Huang and Y. Fang, Synthesis of hierarchical SAPO-11 via seeded crystallization, *Microporous Mesoporous Mater.*, 2015, **218**, 24–32.

15 B. B. Gao, M. Yang, Y. Y. Qiao, J. Z. Li, X. Xiang, P. F. Wu, Y. X. Wei, S. T. Xu, P. Tian and Z. M. Liu, A Low-Temperature Approach to Synthesize Low-Silica SAPO-34 Nanocrystals and their Application in the Methanol-to-Olefins (MTO) Reaction, *Catal. Sci. Technol.*, 2016, **6**, 7569–7578.

16 Q. Sun, N. Wang, R. Bai, X. Chen and J. Yu, Seeding induced nano-sized hierarchical SAPO-34 zeolites: cost-effective synthesis and superior MTO performance, *J. Mater. Chem. A*, 2016, **4**, 14978–14982.

17 S. Zhong, S. Song, B. Wang, N. Bu, X. Ding, R. Zhou and W. Jin, Fast preparation of ERI-structure AlPO-17 and SAPO-17 in the presences of isomorphous and heterogeneous seeds, *Microporous Mesoporous Mater.*, 2018, **263**, 11–20.

18 M. Davis, Ordered porous materials for emerging applications, *Nature*, 2002, **417**, 813–821.

19 M. Y. Kim, K. Lee and M. Choi, Cooperative effects of secondary mesoporosity and acid site location in Pt/SAPO-11 on n-dodecane hydroisomerization selectivity, *J. Catal.*, 2014, **319**, 232–238.

20 M. Yang, B. Li, M. B. Gao, S. F. Lin, Y. Wang, S. T. Xu, X. B. Zhao, P. Guo, Y. X. Wei, M. Ye, P. Tian and Z. M. Liu, High Propylene Selectivity in Methanol Conversion over a Small Pore SAPO Molecular Sieve with Ultra-Small Cage, *ACS Catal.*, 2020, **10**, 3741–3749.

21 X. N. Liu, Y. Cao, N. N. Yan, C. Ma, L. Cao, P. Guo, P. Tian and Z. M. Liu, Cu-SAPO-17: A novel catalyst for selective catalytic reduction of NO_x, *Chin. J. Catal.*, 2020, **41**, 1715–1722.

22 N. Yan, C. Ma, Y. Cao, X. Liu, L. Cao, P. Guo, P. Tian and Z. Liu, Rational Design of a Novel Catalyst Cu-SAPO-42 for NH_3-SCR Reaction, *Small*, 2020, **16**, 2000902.

23 Y. Li and J. Yu, Emerging applications of zeolites in catalysis, separation and host-guest assembly, *Nat. Rev. Mater.*, 2021, **6**, 1156–1174.

24 P. Tian, Y. X. Wei, M. Ye and Z. M. Liu, Methanol to Olefins (MTO): from Fundamentals to Commercialization, *ACS Catal.*, 2015, **5**, 1922–1938.

25 M. Yang, D. Fan, Y. Wei, P. Tian and Z. Liu, Recent Progress in Methanol-to-Olefins (MTO) Catalysts, *Adv. Mater.*, 2019, **31**, 1902181.

26 C. Wang, M. Yang, M. Li, S. Xu, Y. Yang, P. Tian and Z. Liu, A reconstruction strategy to synthesize mesoporous SAPO molecular sieve single crystals with high MTO catalytic activity, *Chem. Commun.*, 2016, **52**, 6463–6466.

27 Q. M. Sun, N. Wang, G. Q. Guo and J. H. Yu, Ultrafast synthesis of nano-sized zeolite SAPO-34 with excellent MTO catalytic performance, *Chem. Commun.*, 2015, **51**, 16397–16400.

28 Z. D. Liu, T. Wakihara, N. Nomura, T. Matsuo, C. Anand, S. P. Elangovan, Y. Yanaba, T. Yoshikawa and T. Okubo, Ultrafast and Continuous Flow Synthesis of Silicoaluminophosphates, *Chem. Mater.*, 2016, **28**, 4840–4847.

29 Y. Jin, Q. Sun, G. Qi, C. Yang, J. Xu, F. Chen, X. Meng, F. Deng and F. S. Xiao, Solvent-free synthesis of silicoaluminophosphate zeolites, *Angew. Chem., Int. Ed.*, 2013, **52**, 9172–9175.

30 G. Chen, Q. Sun and J. Yu, Nanoseed-assisted synthesis of nano-sized SAPO-34 zeolites using morpholine as the sole template with superior MTO performance, *Chem. Commun.*, 2017, **53**, 13328–13331.

31 Q. Sun, N. Wang, R. Bai, G. Chen, Z. Shi, Y. Zou and J. Yu, Mesoporogen-Free Synthesis of Hierarchical SAPO-34 with Low Template Consumption and Excellent Methanol-to-Olefin Conversion, *ChemSusChem*, 2018, **11**, 3812–3820.

32 M. Yang, P. Tian, C. Wang, Y. Yuan, Y. Yang, S. Xu, Y. He and Z. Liu, A Top-Down Approach to Prepare Silicoaluminophosphate Molecular Sieve Nanocrystals with Improved Catalytic Activity, *Chem. Commun.*, 2014, **50**, 1845–1847.

33 P. F. Wu, M. Yang, L. J. Sun, S. Zeng, S. T. Xu, P. Tian and Z. M. Liu, Synthesis of nanosized SAPO-34 with the assistance of bifunctional amine and seeds, *Chem. Commun.*, 2018, **54**, 11160–11163.

34 P. F. Wu, M. Yang, W. N. Zhang, S. T. Xu, P. Guo, P. Tian and Z. M. Liu, Synthesis of SAPO-34 Nanoaggregates with the Assistance of an Inexpensive Three-in-One Non-surfactant Organosilane, *Chem. Commun.*, 2017, **53**, 4985–4988.

35 S. X. Tian, G. Yue, Y. Li, Y. P. Xue and W. P. Zhu, Synthesis of SAPO-34 Molecular Sieve in Presence of Crystal Seed, *China Pet. Process. Petrochem. Technol.*, 2009, **38**, 1276–1280.

36 Z. F. Wu, J. W. Song, Y. Y. Ji, L. M. Ren and F. S. Xiao, Organic Template-Free Synthesis of ZSM-34 Zeolite from an Assistance of Zeolite L Seeds Solution, *Chem. Mater.*, 2008, **20**, 357–359.

37 K. Itabashi, Y. Kamimura, K. Iyoki, A. Shimojima and T. Okubo, A working hypothesis for broadening framework types of zeolites in seed-assisted synthesis without organic

structure-directing agent, *J. Am. Chem. Soc.*, 2012, **134**, 11542–11549.

38 R. Jain and J. D. Rimer, Seed-Assisted zeolite synthesis: The impact of seeding conditions and interzeolite transformations on crystal structure and morphology, *Microporous Mesoporous Mater.*, 2020, **300**, 110174.

39 J. Zhang, Y. Y. Chu, X. Liu, H. Xu, X. J. Meng, Z. C. Feng and F. S. Xiao, Interzeolite transformation from FAU to CHA and MFI zeolites monitored by UV Raman spectroscopy, *Chin. J. Catal.*, 2019, **40**, 1854–1859.

40 J. Zhang, Y. Y. Chu, F. Deng, Z. C. Feng, X. J. Meng and F. S. Xiao, Evolution of D6R units in the interzeolite transformation from FAU, MFI or *BEA into AEI: transfer or reassembly?, *Inorg. Chem. Front.*, 2020, **7**, 2204–2211.

41 L. Wang, P. Tian, Y. Yuan, M. Yang, D. Fan, H. Zhou, W. Zhu, S. Xu and Z. Liu, Seed-assisted synthesis of high silica ZSM-35 through interface-induced growth over MCM-49 seeds, *Microporous Mesoporous Mater.*, 2014, **196**, 89–96.

42 R. Wu, J. Han, Y. Wang, M. Chen, P. Tian, X. Zhou, J. Xu, J. Zhang and W. Yan, Exclusive SAPO-seeded synthesis of ZK-5 zeolite for selective synthesis of methylamines, *Inorg. Chem. Front.*, 2022, **9**, 5766–5773.

43 H. Zhang, B. Wang and W. Yan, The structure-directing role of heterologous seeds in the synthesis of zeolite, *Green Energy Environ.*, 2023, DOI: **10.1016/j.gee.2023.02.005**.

44 D. L. Zhu, L. Y. Wang, W. N. Zhang, D. Fan, J. Z. Li, W. H. Cui, S. J. Huang, S. T. Xu, P. Tian and Z. M. Liu, Realizing Fast Synthesis of High-Silica Zeolite Y with Remarkable Catalytic Performance, *Angew. Chem., Int. Ed.*, 2022, e202117698, DOI: **10.1002/anie.202117698**.

45 X. S. Zhang, M. Yang, P. Tian and Z. M. Liu, Progress in Seed-assisted Synthesis of (Silico)Aluminophosphate Molecular Sieves, *Chem. Res. Chin. Univ.*, 2022, **38**, 1–8.

46 T. Zheng, P. He, R. Zhang, X. Meng, Y. Yue, H. Liu, Z. Liu, C. Xu and H. Liu, Seed-assisted synthesis of SAPO-34 zeolites: Genetic effect of seeds, *J. Taiwan Inst. Chem. Eng.*, 2022, **131**, 104211.

47 Z. Yan, B. Chen and Y. Huang, A Solid-State NMR Study of the Formation of Molecular Sieve SAPO-34, *Solid State Nucl. Magn. Reson.*, 2009, **35**, 49–60.

48 L. Zhang, J. Bates, D. Chen, H. Nie and Y. Huang, Investigations of Formation of Molecular Sieve SAPO-34, *J. Phys. Chem. C*, 2011, **115**, 22309–22319.

49 L. Zhang and Y. N. Huang, Crystallization and Catalytic Properties of Molecular Sieve SAPO-34 by a Vapor-Phase Transport Method, *J. Mater. Chem. A*, 2015, **3**, 4522–4529.

50 S. Ahn, H. Lee and S. Hong, Crystallization Mechanism of Cage-Based, Small-Pore Molecular Sieves: A Case Study of CHA and LEV Structures, *Chem. Mater.*, 2017, **29**, 5583–5590.

51 G. Liu, P. Tian, Y. Zhang, J. Li, L. Xu, S. Meng and Z. Liu, Synthesis of SAPO-34 templated by diethylamine: Crystallization process and Si distribution in the crystals, *Microporous Mesoporous Mater.*, 2008, **114**, 416–423.

52 P. Tian, B. Li, S. T. Xu, X. Su, D. H. Wang, L. Zhang, D. Fan, Y. Qi and Z. M. Liu, Investigation of the Crystallization Process of SAPO-35 and Si Distribution in the Crystals, *J. Phys. Chem. C*, 2013, **117**, 4048–4056.

53 D. Schwalbe-Koda, Z. Jensen, E. Olivetti and R. Gomez-Bombarelli, Graph similarity drives zeolite diffusionless transformations and intergrowth, *Nat. Mater.*, 2019, **18**, 1177–1181.

54 X. Zhang, M. Yang, L. Wang, J. Han, C. Lou, S. Xu, Y. Zhang, R. Wu, P. Tian and Z. Liu, Recognizing the Minimum Structural Units Driving the Crystallization of SAPO-34 in a Top-Down Process, *Chem. – Eur. J.*, 2022, e202203886, DOI: **10.1002/chem.202203886**.

55 Y. Huang, D. Machado and C. Kirby, A Study of the Formation of Molecular Sieve SAPO-44, *J. Phys. Chem. B*, 2004, **108**, 1855–1865.

56 B. Arstad, A. Lind, J. Cavka, K. Thorshaug, D. Akporiaye, D. Wragg, H. Fjellvag, A. Gronvold and T. Fuglerud, Structural changes in SAPO-34 due to hydrothermal treatment. A NMR, XRD, and DRIFTS study, *Microporous Mesoporous Mater.*, 2016, **225**, 421–431.

57 D. Verboekend, M. Milina and J. Perez-Ramirez, Hierarchical Silicoaluminophosphates by Postsynthetic Modification: Influence of Topology, Composition, and Silicon Distribution, *Chem. Mater.*, 2014, **26**, 4552–4562.

58 Y. Qiao, M. Yang, B. Gao, L. Wang, P. Tian, S. Xu and Z. Liu, Creation of Hollow SAPO-34 Single Crystals via Alkaline or Acid Etching, *Chem. Commun.*, 2016, **52**, 5718–5721.

59 B. Li, P. Tian, Y. Qi, L. Zhang, S. Xu, X. Su, D. Fan and Z. Liu, Study of crystallization process of SAPO-11 molecular sieve, *Chin. J. Catal.*, 2013, **34**, 593–603.